Supporting Information

Synthesis and Characterization of Complexes Constructed from 5-(benzimidazole-1-yl)isophthalic Acid and Highly Selective Fluorescence Detection of Fe(Ⅲ) and Cr(Ⅵ) in Water

Bin Zhu[b], Guimei Huang[a], Yanni He[a], Jisheng Xie[a], Tao He[a], Junli Wang[a]*, Ziao Zong[a]*

[a] School of Laboratory Medicine, Youjiang Medical University for Nationalities, Baise, 533000 Guangxi, China

[b] College of Chemistry and Chemical Engineering, Ocean University of China, Qingdao, 266100, Shandong, China

Section 1. Materials and physical measurements

All reagents and solvents were purchased from Jinan Henghua Sci. Tec. Co. Ltd., and used without further purification. Infrared spectra were recorded on the Bruker TENSOR Ⅱ spectrometer in the 4000-400 cm^{-1} region by KBr pellets. Elemental analysis of C, H, N were performed in a model 2400 PerkinElmer analyzer. Thermogravimetric (TG) analyses were measured on a Perkin-Elmer TGA-7 thermogravimetric analyzer under N_2 conditions from room temperature to 800 ℃ with a heating rate of 10 ℃ min^{-1}. The surface area was determined using Brunauer–Emmett–Teller (BET) measured using nitrogen adsorption–desorption method at a low-temperature on a Micromeritics ASAP 2020 (Micromeritics USA). The X-ray powder diffractions (PXRD) were collected on an Enraf-Nonius CAD-4 X-ray single crystal

diffractometer with Cu-Kα radiation. Topological analysis was performed and confirmed by the Topos program and the Systre software.

Section 2. X-ray crystal structure determination

The single crystal X-ray data of complexes **1-4** were collected at low temperature on a Bruker Apex Smart CCD diffractometer, equipped with graphite monochromatic Mo-Kα radiation (λ = 0.71073Å), and the scanning mode was ω-2θ. The crystal structure was solved by the direct method and refined by using the full matrix least squares method (on F^2) on the SHELXL-2015 program. Hydrogen atoms attached to carbon atoms were placed in geometrically calculated positions, and all non-hydrogen atoms were refined by the Fourier synthesis method. The solvent masking procedure as implemented in Olex2 was used to remove the electronic contribution of non-coordinated solvent molecules from the refinement. TWINABS-2012/1 (Bruker,2012) was used for absorption correction.

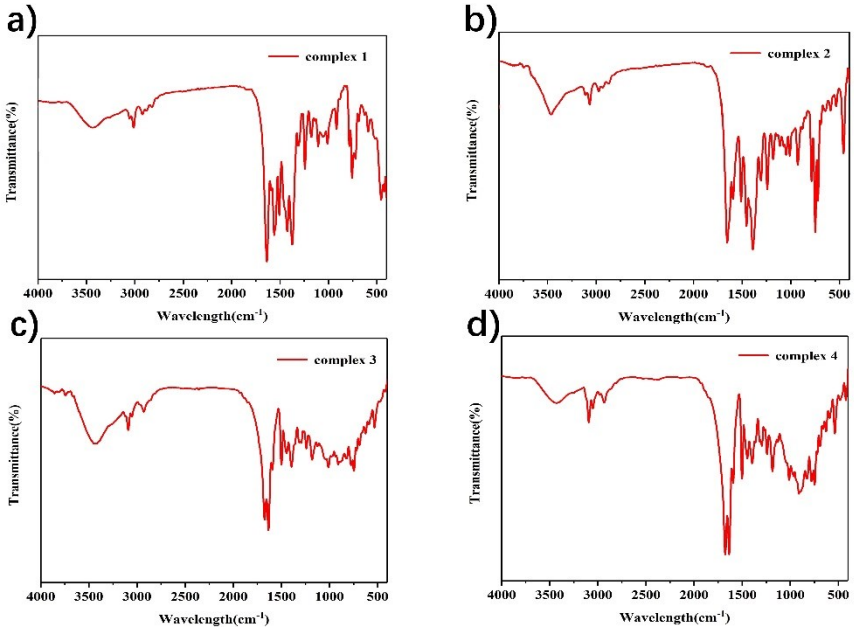

Figure S1. The FT-IR spectra of (a) complex **1**; (b) complex **2**; (c) complex **3**; (d) complex **4**.

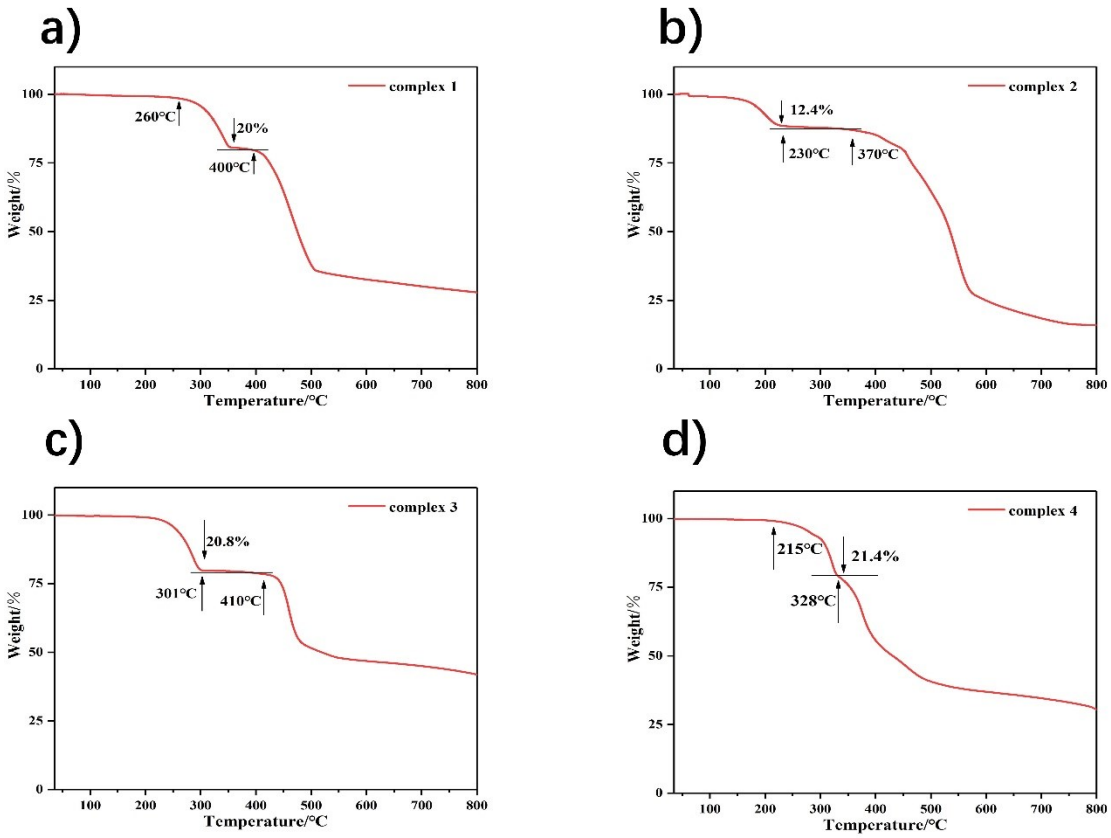

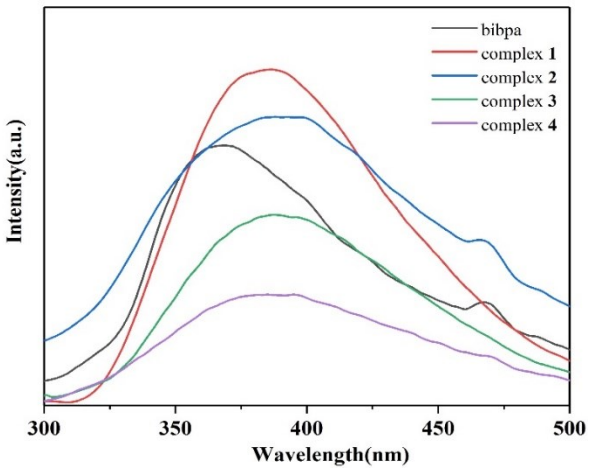

Figure S3. The solid-state fluorescence spectra of solid samples of **1-4** and ligand.

Figure S2. Th

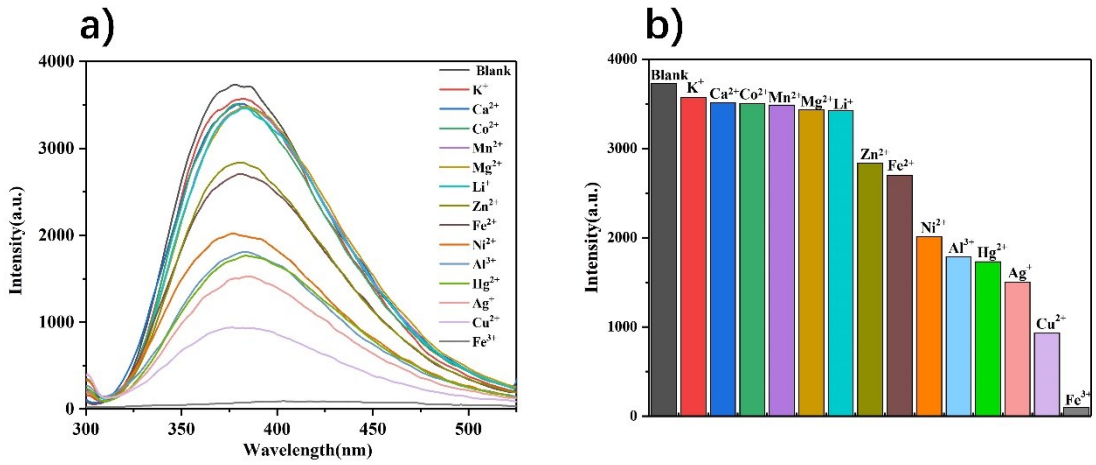

Figure S4. Fluorescence intensity of complex **1** immersed in 1 mM aqueous solution of di□erent mate ions.

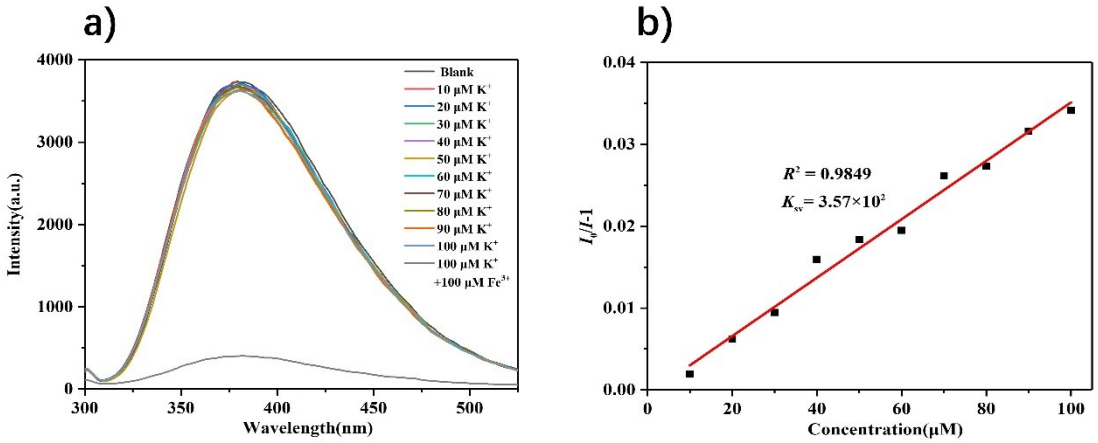

Figure S5. (a) Fluorescence spectra of complex **1** in the presence of K^+ and adding equivalent Fe^{3+} (100 μM)); (b) S−V plot of complex **1** upon incremental addition of K^+ (0-100 μM)).

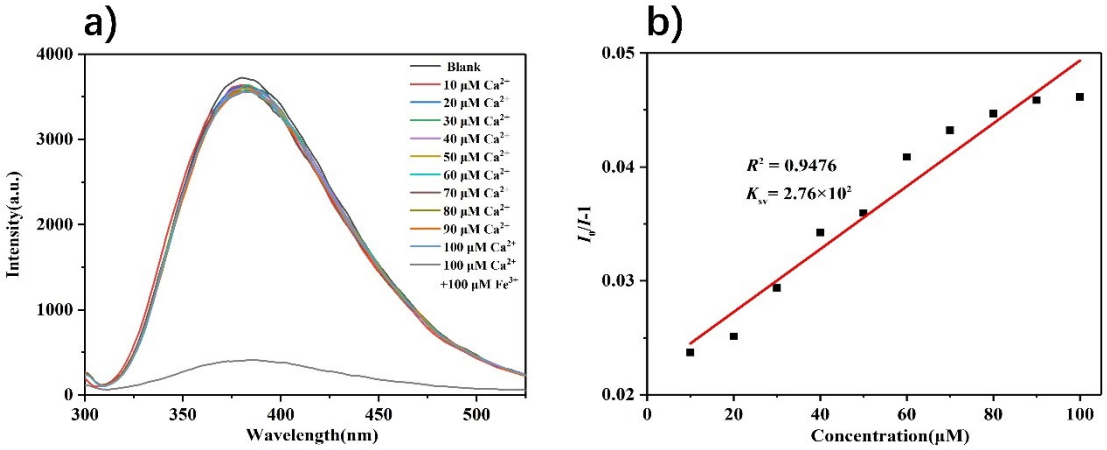

Figure S6. (a) Fluorescence spectra of complex **1** in the presence of Ca^{2+} and adding equivalent Fe^{3+} (100 μM)); (b) S−V plot of complex **1** upon incremental addition of Ca^{2+} (0-100 μM)).

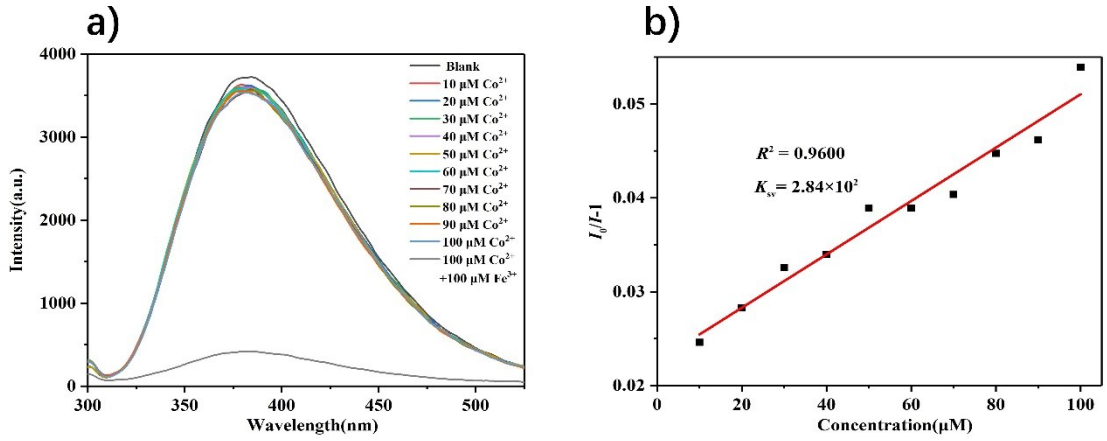

Figure S7. (a) Fluorescence spectra of complex **1** in the presence of Co^{2+} and adding equivalent Fe^{3+} (100 μM)); (b) S−V plot of complex **1** upon incremental addition of Co^{2+} (0-100 μM)).

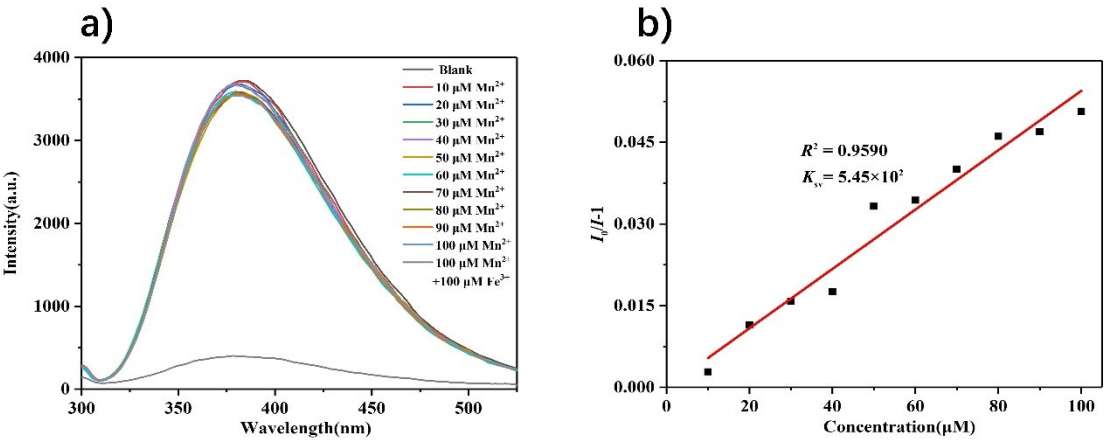

Figure S8. (a) Fluorescence spectra of complex **1** in the presence of Mn^{2+} and adding equivalent Fe^{3+} (100 μM)); (b) S−V plot of complex **1** upon incremental addition of Mn^{2+} (0-100 μM)).

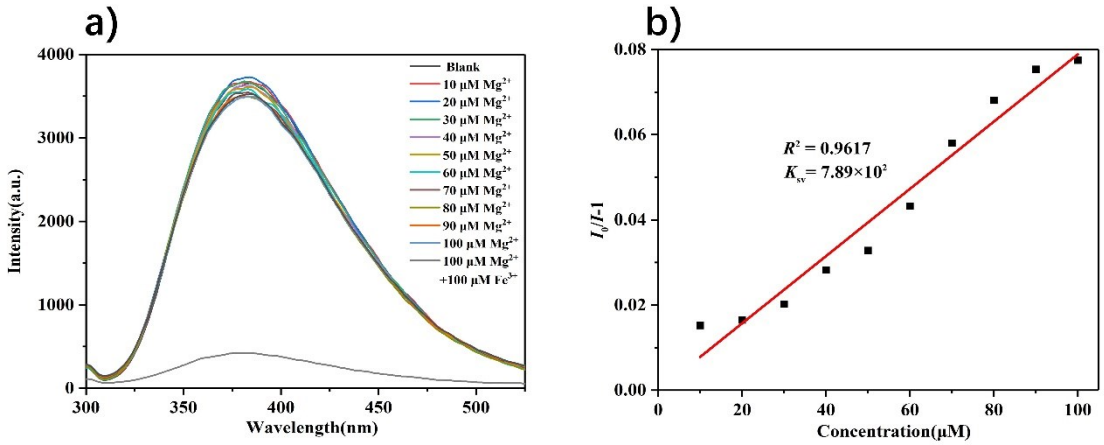

Figure S9. (a) Fluorescence spectra of complex **1** in the presence of Mg^{2+} and adding equivalent Fe^{3+} (100 μM)); (b) S−V plot of complex **1** upon incremental addition of Mg^{2+} (0-100 μM)).

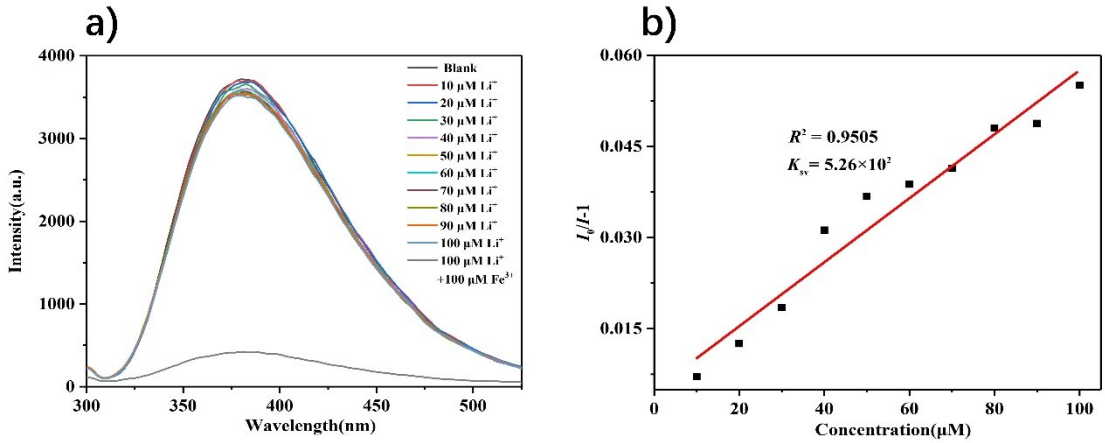

Figure S10. (a) Fluorescence spectra of complex **1** in the presence of Li^{+} and adding equivalent Fe^{3+} (100 μM)); (b) S−V plot of complex **1** upon incremental addition of Li^{+} (0-100 μM)).

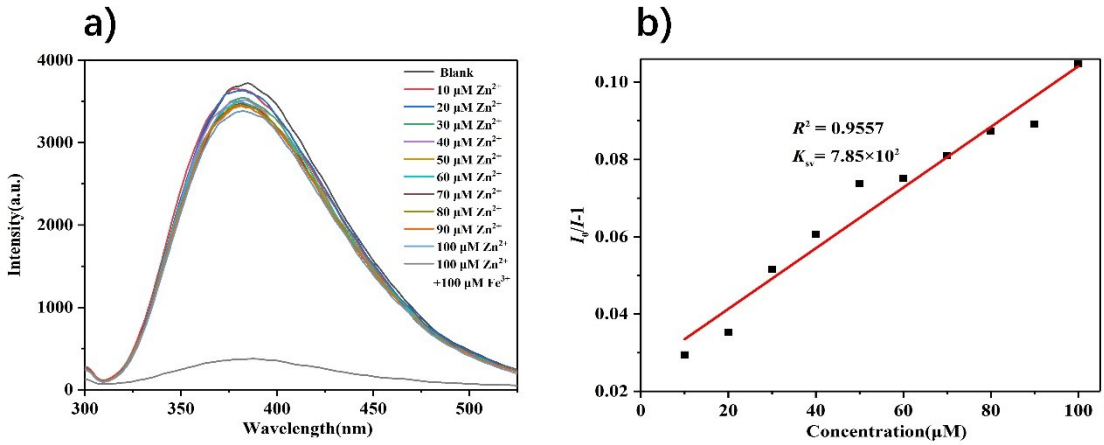

Figure S11. (a) Fluorescence spectra of complex **1** in the presence of Zn^{2+} and adding equivalent Fe^{3+} (100 μM)); (b) S−V plot of complex **1** upon incremental addition of Zn^{2+} (0-100 μM)).

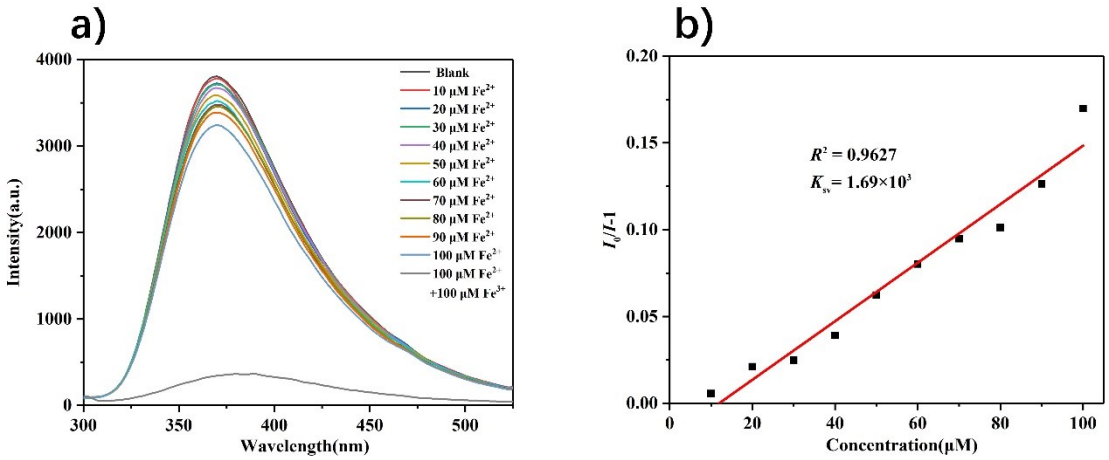

Figure S12. (a) Fluorescence spectra of complex **1** in the presence of Fe^{2+} and adding equivalent Fe^{3+} (100 μM)); (b) S−V plot of complex **1** upon incremental addition of Ni^{2+} (0-100 μM)).

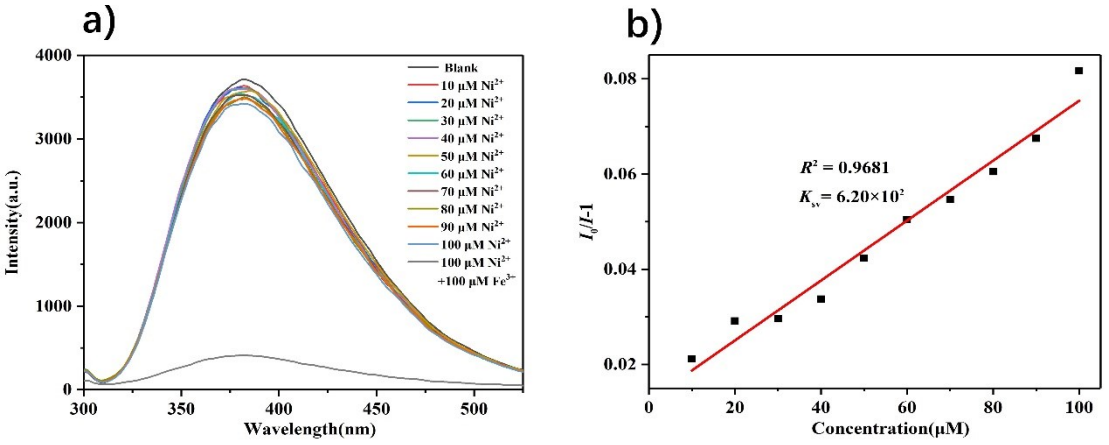

Figure S13. (a) Fluorescence spectra of complex **1** in the presence of Ni^{2+} and adding equivalent Fe^{3+} (100 μM)); (b) S−V plot of complex **1** upon incremental addition of Ni^{2+} (0-100 μM)).

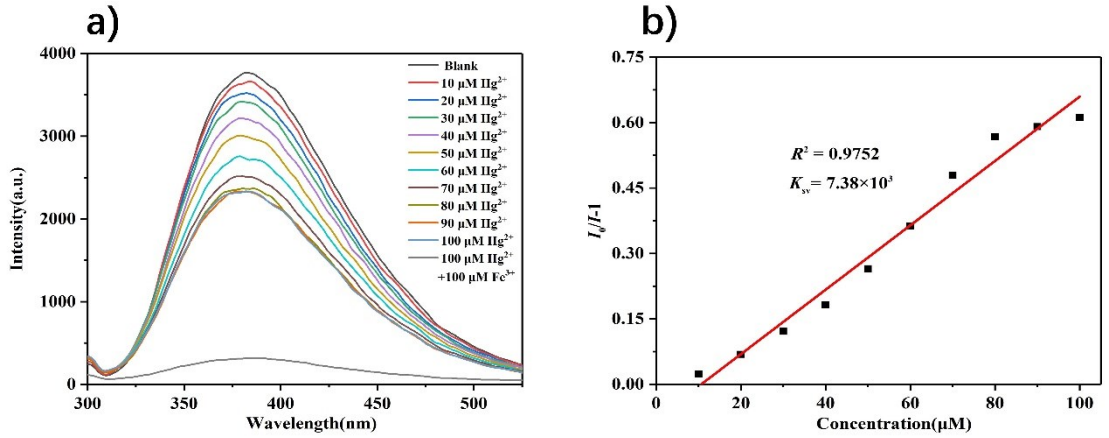

Figure S14. (a) Fluorescence spectra of complex **1** in the presence of Hg^{2+} and adding equivalent Fe^{3+} (100 μM)); (b) S−V plot of complex **1** upon incremental addition of Hg^{2+} (0-100 μM)).

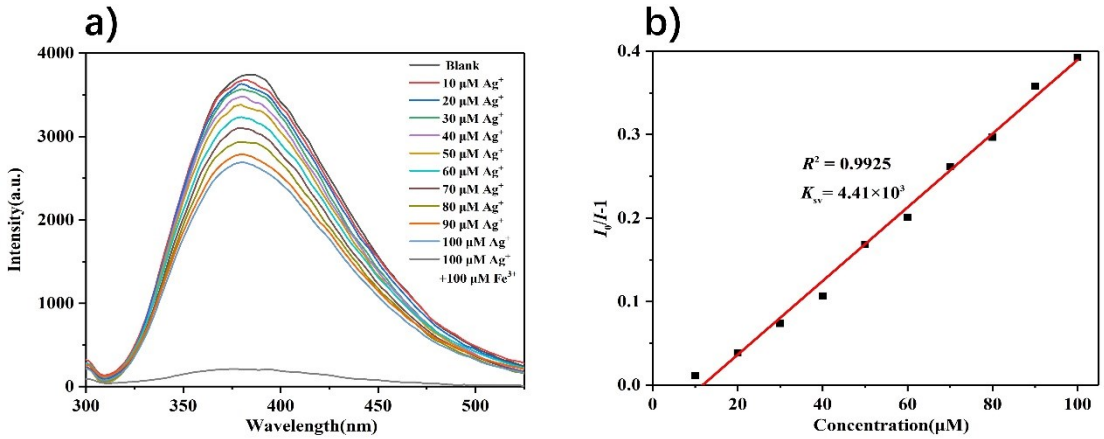

Figure S15. (a) Fluorescence spectra of complex **1** in the presence of Ag^{+} and adding equivalent Fe^{3+} (100 μM)); (b) S−V plot of complex **1** upon incremental addition of Ag^{+} (0-100 μM)).

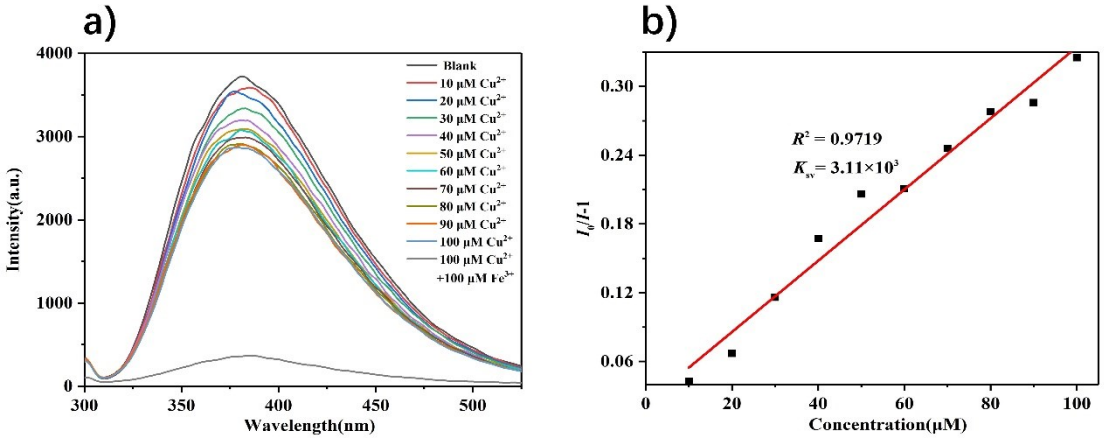

Figure S16. (a) Fluorescence spectra of complex **1** in the presence of Cu^{2+} and adding equivalent Fe^{3+} (100 μM)); (b) S−V plot of complex **1** upon incremental addition of Hg^{2+} (0-100 μM)).

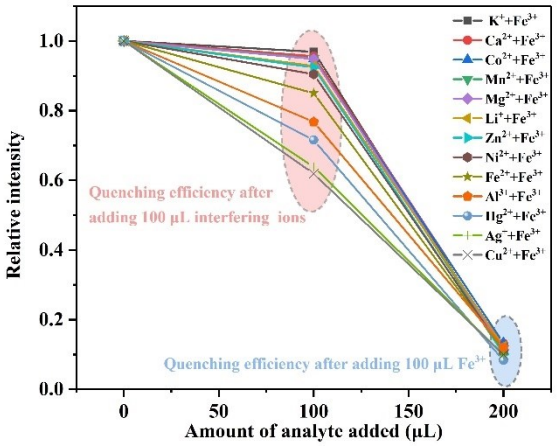

Figure S17. Interference plot of decrease in fluorescence intensities after adding Fe^{3+} in the presence of different mate ions (100 μM).

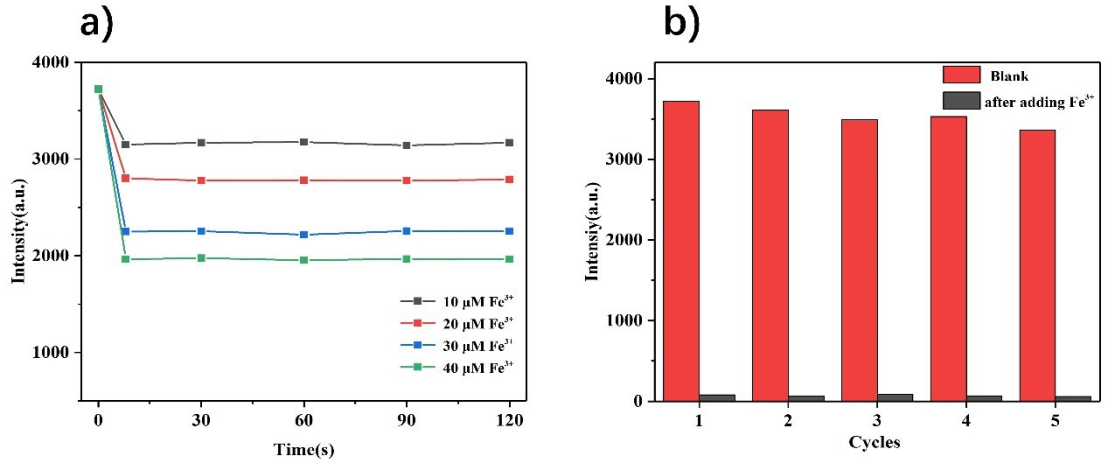

Figure S18. (a) The line chart of the complex **1** fluorescence intensity *versus* time as adding the different concentration of Fe^{3+}; (b) the cycle stability of **1** for the detection of Fe^{3+}.

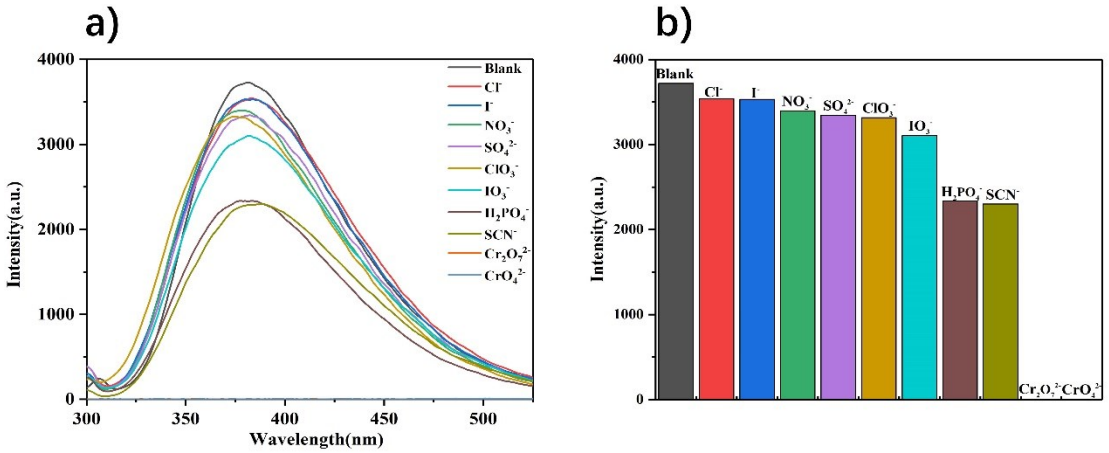

Figure S19. Fluorescence intensity of complex **1** immersed in 1 mM aqueous solution of di□erent anions.

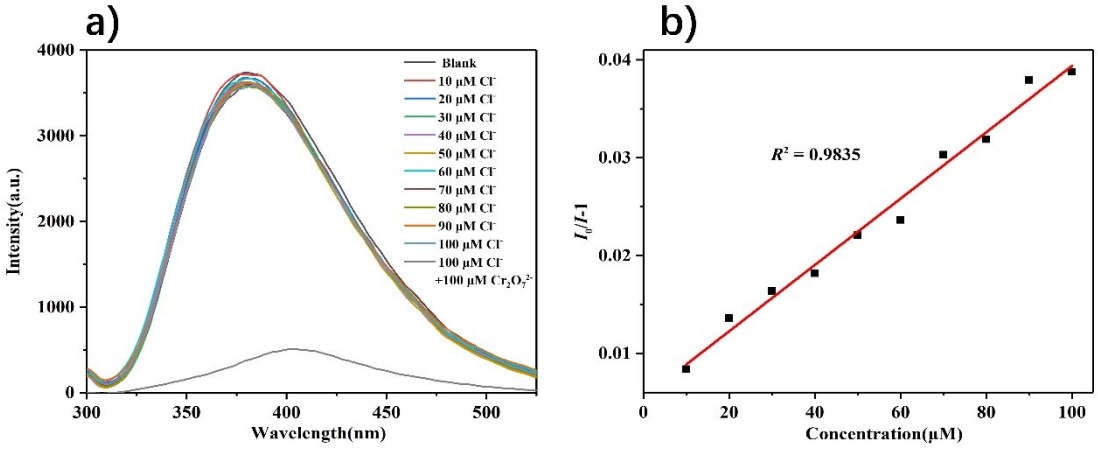

Figure S20. (a) Fluorescence spectra of complex **1** in the presence of Cl^- and adding equivalent $Cr_2O_7^{2-}$ (100 μM); (b) S−V plot of complex **1** upon incremental addition of Cl^- (0-100 μM)).

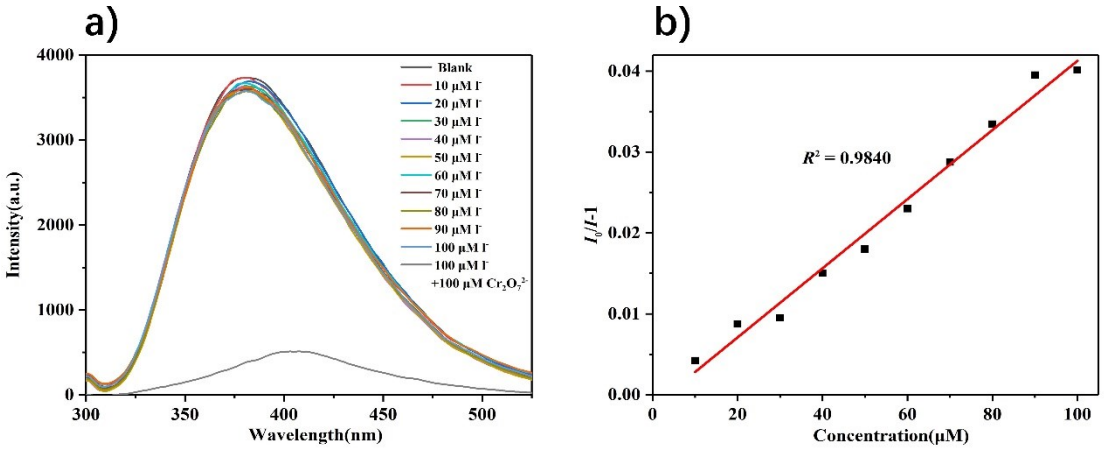

Figure S21. (a) Fluorescence spectra of complex **1** in the presence of I^- and adding equivalent $Cr_2O_7^{2-}$ (100 μM); (b) S−V plot of complex **1** upon incremental addition of I^- (0-100 μM)).

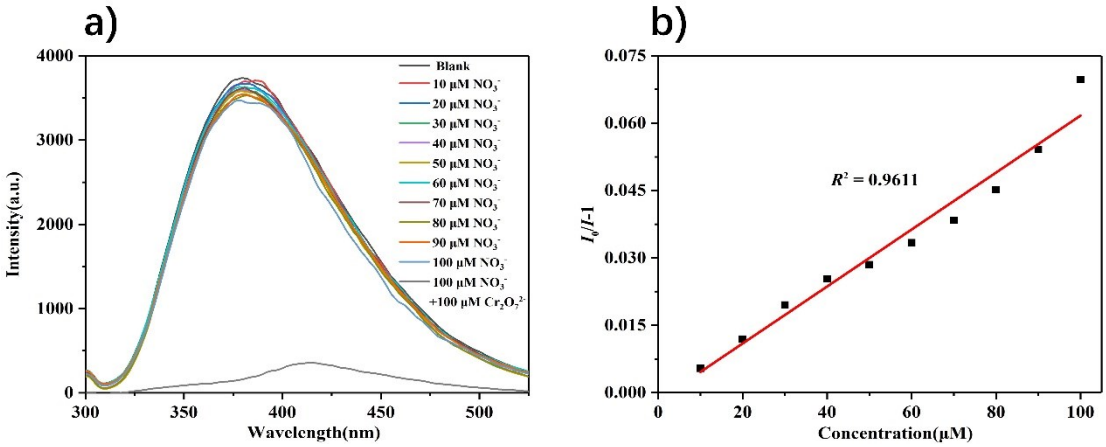

Figure S22. (a) Fluorescence spectra of complex **1** in the presence of NO_3^- and adding equivalent $Cr_2O_7^{2-}$ (100 μM); (b) S−V plot of complex **1** upon incremental addition of NO_3^- (0-100 μM)).

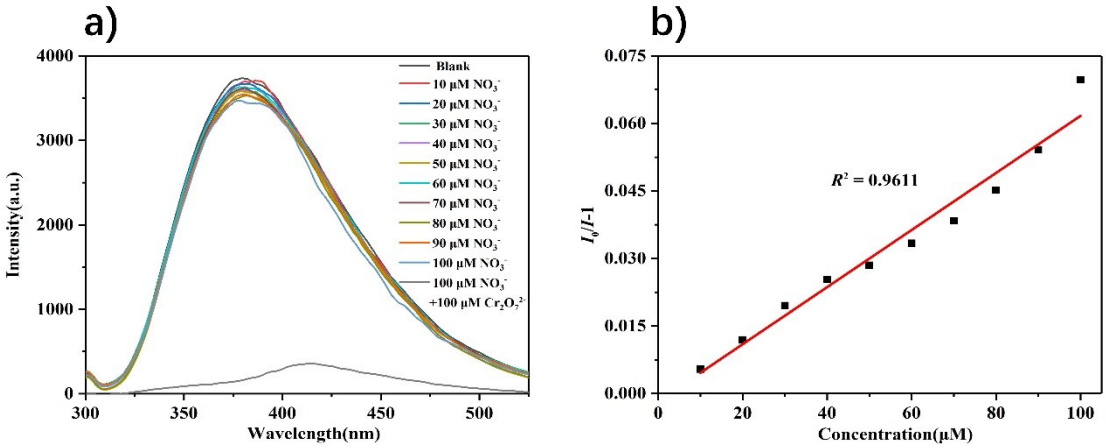

Figure S23. (a) Fluorescence spectra of complex **1** in the presence of SO_4^{2-} and adding equivalent $Cr_2O_7^{2-}$ (100 μM); (b) S−V plot of complex **1** upon incremental addition of SO_4^{2-} (0-100 μM)).

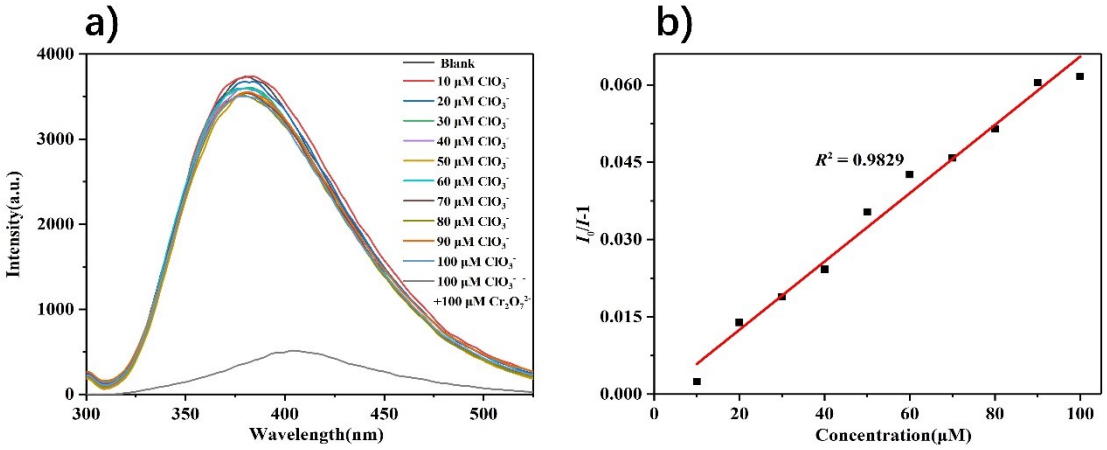

Figure S24. (a) Fluorescence spectra of complex **1** in the presence of ClO_3^- and adding equivalent $Cr_2O_7^{2-}$ (100 μM); (b) S−V plot of complex **1** upon incremental addition of ClO_3^- (0-100 μM)).

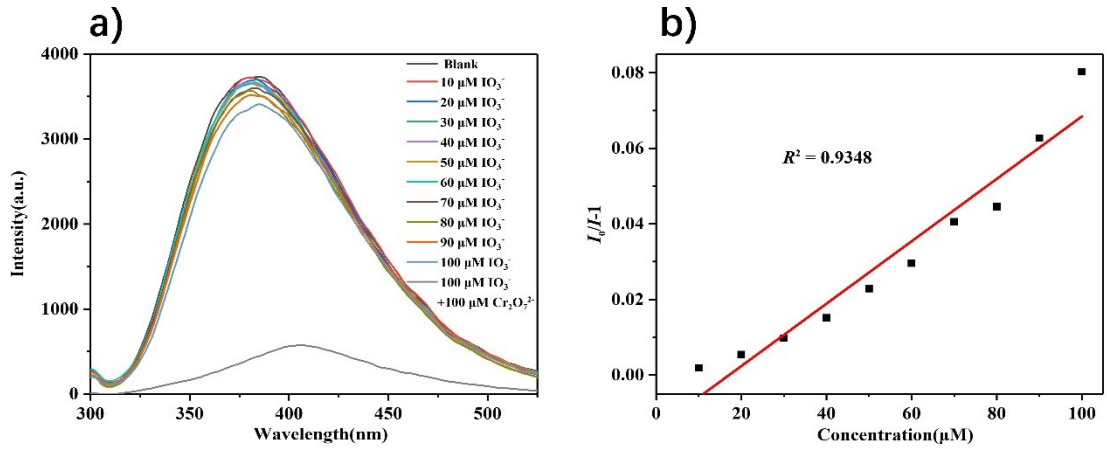

Figure S25. (a) Fluorescence spectra of complex **1** in the presence of IO_3^- and adding equivalent $Cr_2O_7^{2-}$ (100 μM); (b) S−V plot of complex **1** upon incremental addition of IO_3^- (0-100 μM)).

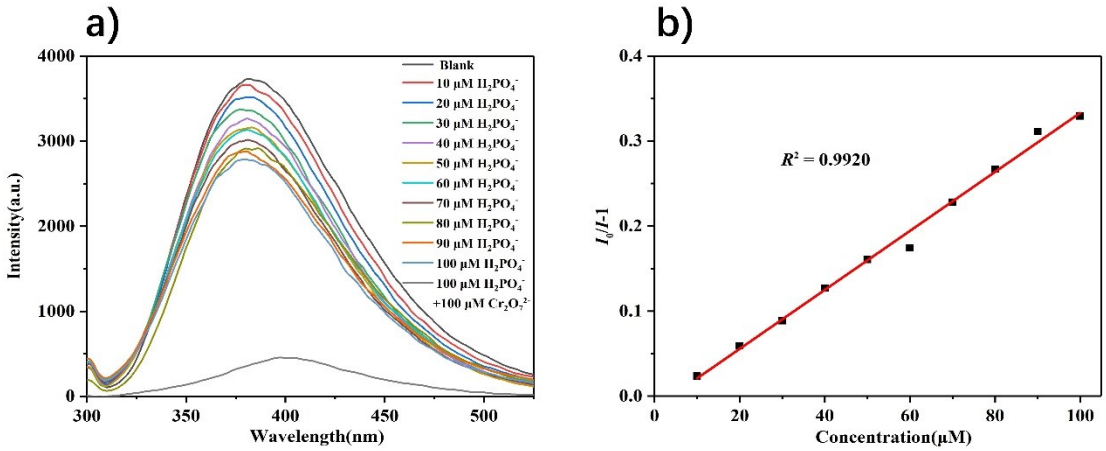

Figure S26. (a) Fluorescence spectra of complex **1** in the presence of $H_2PO_4^-$ and adding equivalent $Cr_2O_7^{2-}$ (100 μM); (b) S−V plot of complex **1** upon incremental addition of $H_2PO_4^-$ (0-100 μM)).

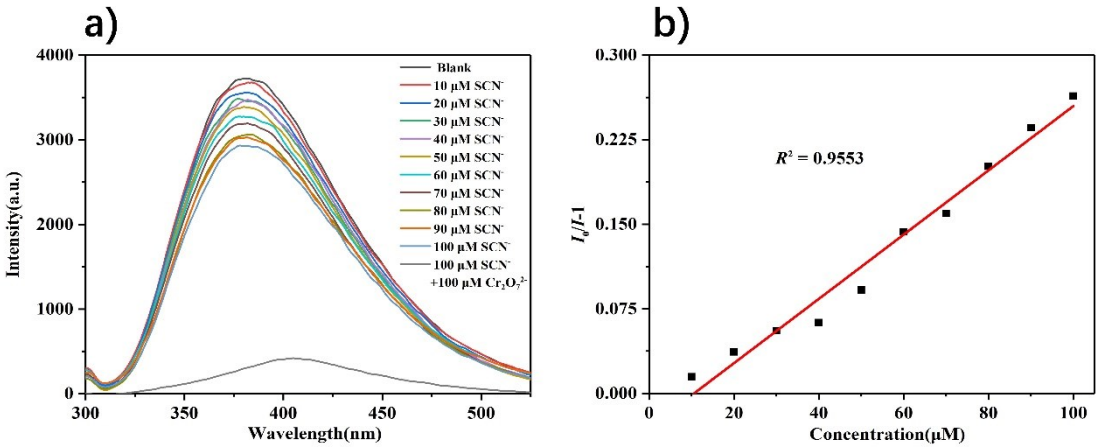

Figure S27. (a) Fluorescence spectra of complex **1** in the presence of SCN^- and adding equivalent $Cr_2O_7^{2-}$ (100 μM); (b) S−V plot of complex **1** upon incremental addition of SCN^- (0-100 μM)).

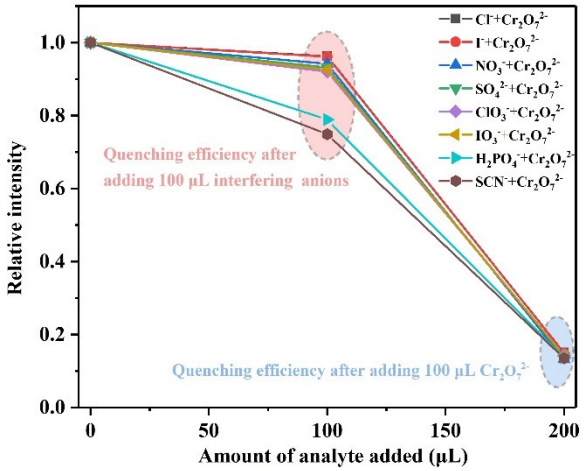

Figure S28. Interference plot of decrease in fluorescence intensities after adding $Cr_2O_7^{2-}$ in the presence of different anions (100 μM).

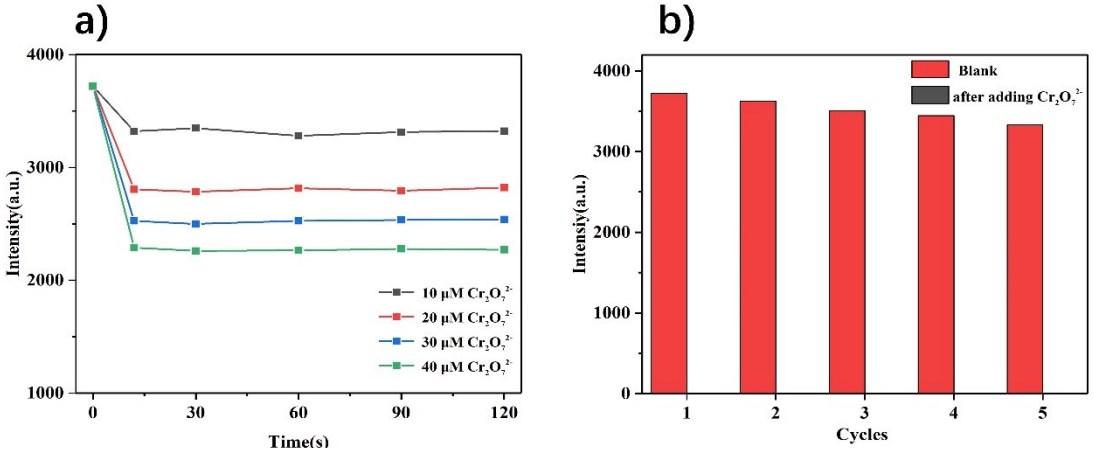

Figure S29. (a) The line chart of the complex **1** fluorescence intensity *versus* time as adding the different concentration of $Cr_2O_7^{2-}$; (b) the cycle stability of **1** for the detection of $Cr_2O_7^{2-}$.

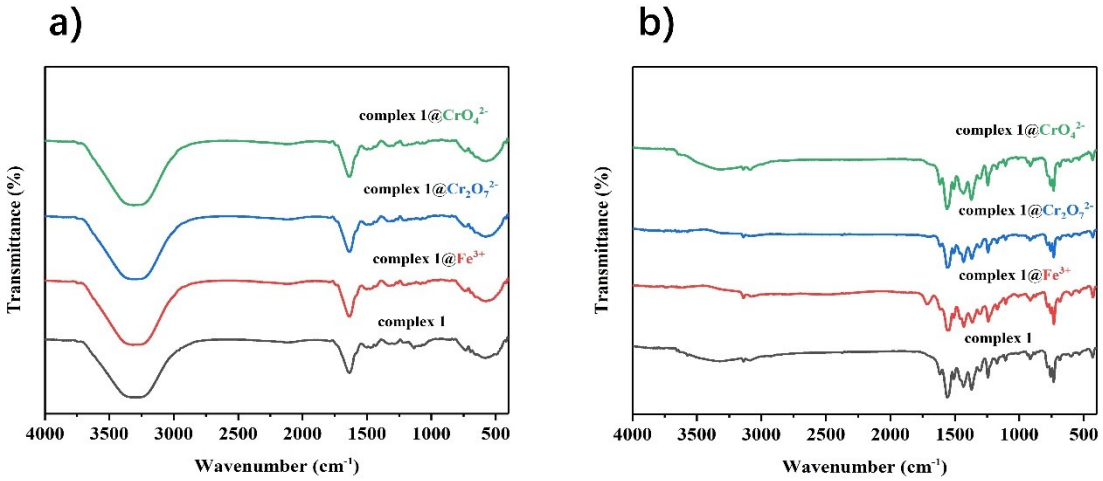

Figure S30. (a) Liquid IR spectra of suspensions of complex **1**, complex **1**@Fe^{3+}, complex **1**@$Cr_2O_7^{2-}$ and complex **1**@CrO_4^{2-}; (b) IR spectra of powder of complex **1** and that recovered from the suspensions containing Fe^{3+}, $Cr_2O_7^{2-}$ and CrO_4^{2-}.

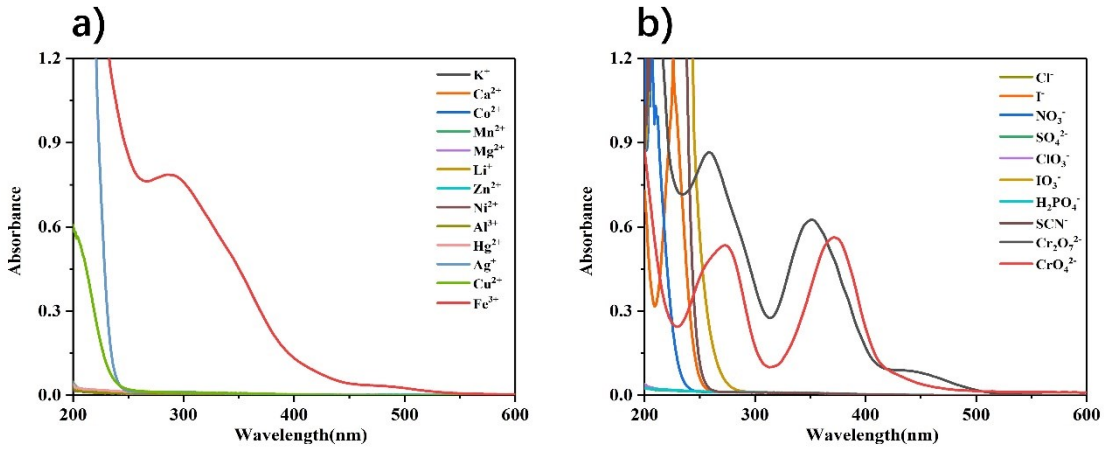

Figure S31. UV-vis absorption spectra of di□erent (a) mate ions; (b) anions.

TABLE S1. Selected bond lengths (Å) and angles (deg) for 1-4.

Complex **1**			
Cd1—O4^{ii}	2.225 (2)	Cd1—O1	2.208 (2)
Cd1—O2^{i}	2.234 (2)	Cd1—O3^{iii}	2.254 (2)
Cd1—N2^{iv}	2.218 (3)		
O4^{ii}—Cd1—O2^{i}	82.73 (10)	O1—Cd1—O3^{iii}	86.17 (10)
O4^{ii}—Cd1—O3^{iii}	154.39 (10)	O1—Cd1—N2^{iv}	106.73 (10)
O2^{i}—Cd1—O3^{iii}	87.97 (10)	N2^{iv}—Cd1—O4^{ii}	99.94 (10)
O1—Cd1—O4^{ii}	92.19 (10)	N2^{iv}—Cd1—O2^{i}	98.39 (10)
O1—Cd1—O2^{i}	154.88 (10)	N2^{iv}—Cd1—O3^{iii}	105.02 (10)
Complex **2**			
Zn1—O1	2.013 (4)	Zn2—O8^{v}	2.052 (4)
Zn1—O2^{i}	2.038 (4)	Zn2—O9^{vi}	2.018 (4)
Zn1—O3^{ii}	2.044 (4)	Zn2—O10^{vii}	2.023 (4)
Zn1—N3	2.027 (5)	Zn2—N1	2.001 (5)
Zn1—O4^{iii}	2.075 (4)	Zn2—O7^{viii}	2.055 (4)
O1—Zn1—O2^{i}	156.96 (19)	O8^{v}—Zn2—O7^{viii}	157.47 (18)
O1—Zn1—O3^{ii}	90.38 (18)	O9^{vi}—Zn2—O8^{v}	90.41 (18)
O1—Zn1—N3	105.7 (2)	O9^{vi}—Zn2—O10^{vii}	156.28 (19)
O1—Zn1—O4^{iii}	88.16 (18)	O9^{vi}—Zn2—O7^{viii}	87.79 (18)
O2^{i}—Zn1—O3^{ii}	88.06 (18)	O10^{vii}—Zn2—O8^{v}	88.04 (19)
O2^{i}—Zn1—O4^{iii}	84.57 (19)	O10^{vii}—Zn2—O7^{viii}	84.70 (19)
O3^{ii}—Zn1—O4^{iii}	157.41 (18)	N1—Zn2—O8^{v}	106.35 (19)
N3—Zn1—O2^{i}	96.7 (2)	N1—Zn2—O9^{vi}	107.4 (2)
N3—Zn1—O3^{ii}	106.7 (2)	N1—Zn2—O10^{vii}	95.7 (2)
N3—Zn1—O4^{iii}	95.4 (2)	N1—Zn2—O7^{viii}	95.59 (19)
Complex **3**			

Co1—O3	2.009 (3)	Co1—O4^{i}	2.046 (3)
Co1—O2^{ii}	2.073 (3)	Co1—O1^{iii}	2.028 (3)
Co1—N006^{iv}	2.048 (3)		
O3—Co1—O2^{ii}	87.94 (11)	O4^{i}—Co1—N006^{iv}	92.83 (12)
O3—Co1—O4^{i}	160.02 (12)	O1^{iii}—Co1—O2^{ii}	161.37 (12)
O3—Co1—O1^{iii}	93.17 (11)	O4^{i}—Co1—O2^{ii}	83.65 (11)
O3—Co1—N006^{iv}	105.44 (12)	N006^{iv}—Co1—O2^{ii}	91.01 (11)
O1^{iii}—Co1—O4^{i}	89.20 (12)	O1^{iii}—Co1—N006^{iv}	106.55 (12)
Complex **4**			
Ni1—O4^{i}	2.119 (2)	Ni1—O2^{iv}	2.087 (2)
Ni1—O4^{ii}	2.119 (2)	Ni1—N2^{v}	2.064 (2)
Ni1—O2^{iii}	2.087 (2)	Ni1—N2	2.064 (2)
O4^{ii}—Ni1—O4^{i}	169.58 (11)	N2—Ni1—O4^{i}	84.38 (9)
O2^{iv}—Ni1—O4^{ii}	100.66 (9)	N2—Ni1—O4^{ii}	88.43 (9)
O2^{iii}—Ni1—O4^{i}	100.66 (9)	N2^{v}—Ni1—O2^{iv}	174.52 (10)
O2^{iii}—Ni1—O4^{ii}	86.84 (9)	N2—Ni1—O2^{iv}	89.49 (9)
O2^{iv}—Ni1—O4^{i}	86.84 (9)	N2—Ni1—O2^{iii}	174.52 (10)
O2^{iii}—Ni1—O2^{iv}	88.67 (12)	N2^{v}—Ni1—O2^{iii}	89.49 (9)
N2^{v}—Ni1—O4^{i}	88.44 (9)	N2—Ni1—N2^{v}	92.80 (14)
N2^{v}—Ni1—O4^{ii}	84.38 (9)		

Symmetry codes for complex **1**: (i) -*x*+2, -*y*+1, -*z*+1; (ii) -*x*+2, *y*-1/2, -*z*+3/2; (iii) *x*, -*y*+3/2, *z*-1/2; (iv) *x*+1, *y*, *z*; complex **2**: (i) -*x*, -*y*+2, -*z*+1; (ii) *x*, -*y*+3/2, *z*+1/2; (iii) -*x*, *y*+1/2, -*z*+1/2; (iv) -*x*-1, -*y*+1, -*z*; (v) *x*-1, -*y*+3/2, *z*-1/2; (vi) *x*-1, *y*, *z*-1; (vii) -*x*, -*y*+1, -*z*+1; (viii) -*x*, *y*-1/2, -*z*+1/2; complex **3**: (i) -*x*+2, -*y*+2, -*z*+1; (ii) -*x*+2, *y*+1/2, -*z*+1/2; (iii) *x*, -*y*+3/2, *z*+1/2; (iv) *x*+1, -*y*+3/2, *z*+1/2; complex **4**: (i) -*x*+1, -*y*+1, -*z*+1; (ii) *x*, -*y*+1, *z*+1/2; (iii) -*x*+1, *y*-1, -*z*+3/2; (iv) *x*, *y*-1, *z*; (v) -*x*+1, *y*, -*z*+3/2;

Table S2. A comparison of quenching constants of various MOFs for dual sensing of Fe^{3+} and $CrO4^{2-}/Cr_2O7^{2-}$ ions.

MOF	Analytes	Quenching constant (K_{sv}) (M^{-1})	References
$[Tb_4(L)_6(H_2O)_8]$	Fe^{3+} CrO_4^{2-} $Cr_2O_7^{2-}$	1.88×10^4 3.9×10^3 4.1×10^3	1
$Tb(Hmcd)(H_2O)(DMF)_2]_n$	Fe^{3+} CrO_4^{2-} $Cr_2O_7^{2-}$	7.252×10^3 9.295×10^2 2.7328×10^4	2
Bi-MOF	Fe^{3+} CrO_4^{2-} $Cr_2O_7^{2-}$	2.02×10^4 - 1.95×10^4	3
$[Eu_2(HICA)(BTEC)(H_2O)_2]_n$	Fe^{3+} CrO_4^{2-} $Cr_2O_7^{2-}$	2.028×10^4 1.915×10^4 1.141×10^4	4
$[Zn_2(tpeb)(bpdc)_2]$	Fe^{3+} CrO_4^{2-} $Cr_2O_7^{2-}$	1.326×10^4 1.085×10^4 1.122×10^4	5
$\{[Zn(L)(H_2O)_2]\cdot H_2O\}_n$ $\{[Cd(L)(H_2O)_2]\cdot 4H_2O\}_n$	Fe^{3+} CrO_4^{2-} $Cr_2O_7^{2-}$	1.09×10^5 /4.1×10^4 9.1×10^4 /9.77×10^4 7.2×10^4 /3.03×10^4	6
$\{[Zn_3(mtrb_{)3}(btc)_2]\cdot_3H_2O\}_n$	Fe^{3+} CrO_4^{2-} $Cr_2O_7^{2-}$	6.50×10^3 2.77×10^3 4.62×10^3	7
Zn-MOF	Fe^{3+} CrO_4^{2-} $Cr_2O_7^{2-}$	1.9×10^4 7.81×10^3 9.21×10^3	8

$[Zn_2\{(L)_2(DMF)_2(NO_3)_2\}]\cdot(NO_3)_2$ $[\{Cd_1(L)_2(DMF)_2\}\cdot(NO_3)_2]_n$	Fe^{3+} CrO_4^{2-} -	2.34×10^6 / 6.72×10^5 3.25×10^6 / 6.94×10^5 -	9
$\{[Zn(L8)_{0.5}(bimb)]\cdot 2H_2O\cdot 0.5(CH_3)_2NH\}_n$ $\{[Zn(L8)_{0.5}(bimmb)]\cdot 2H_2O\}_n$ $\{[Zn(L8)_{0.5}(btdpe)]\cdot H_2O\}_n$ $[Zn(L8)_{0.5}(bidpe)]_n$	Fe^{3+} CrO_4^{2-} $Cr_2O_7^{2-}$	6.28×10^4 /5.04×10^4 /5.68×10^4 4.07×10^4 /6.76×10^4 /7.35×10^4 5.1×10^4 /6.47×10^4 /5.55×10^4 4.97×10^4 /5.54×10^4 /6.20×10^4	10
Complex **1**	Fe^{3+} CrO_4^{2-} $Cr_2O_7^{2-}$	2.21×10^4 1.63×10^4 1.73×10^4	This work

References:

1. X. Wang, J.-L. Li, C. Jiang, P. Hu, B. Li, T. Zhang and H.-C. Zhou, *Chemical Communications*, 2018, 54, 13271-13274.
2. X. Li, J. Tang, H. Liu, K. Gao, X. Meng, J. Wu and H. Hou, 2019, 14, 3721-3727.
3. Y. Sun, N. Zhang, Q. L. Guan, C. H. Liu, B. Li, K. Y. Zhang, G. H. Li, Y. H. Xing, F. Y. Bai and L. X. Sun, *Crystal Growth & Design*, 2019, 19, 7217-7229.
4. H. Yu, M. Fan, Q. Liu, Z. Su, X. Li, Q. Pan and X. Hu, *Inorganic Chemistry*, 2020, 59, 2005-2010.
5. B. B. Rath and J. J. Vittal, *Inorganic Chemistry*, 2020, 59, 8818-8826.
6. A.-M. Zhou, H. Wei, W. Gao, J.-P. Liu and X.-M. Zhang, *CrystEngComm*, 2019, 21, 5185-5194.
7. Y.-Q. Zhang, V. A. Blatov, T.-R. Zheng, C.-H. Yang, L.-L. Qian, K. Li, B.-L. Li and B. Wu, *Dalton Transactions*, 2018, 47, 6189-6198.
8. R. Lv, H. Li, J. Su, X. Fu, B. Yang, W. Gu and X. Liu, *Inorganic Chemistry*, 2017, 56, 12348-12356.
9. P. Rani, A. Sharma, A. Husain, G. Kumar, H. Kaur, K. K. Bhasin and G. Kumar, *CrystEngComm*, 2019, 21, 7447-7459.
10. C. Xu, C. Bi, Z. Zhu, R. Luo, X. Zhang, D. Zhang, C. Fan, L. Cui and Y. Fan, *CrystEngComm*, 2019, 21, 2333-2344.